ChemComm

Accepted Manuscript

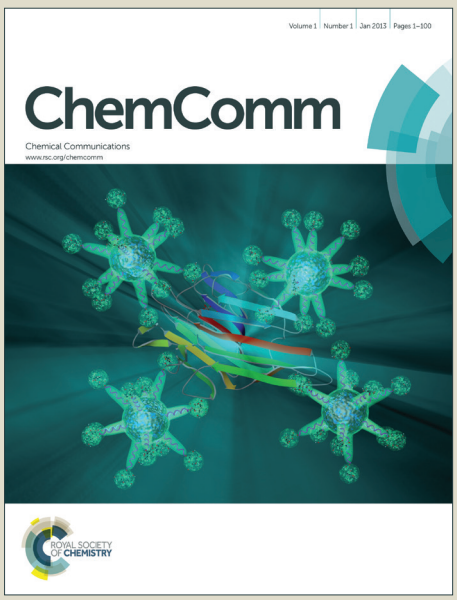

ROYAL SOCIETY OF CHEMISTRY

www.rsc.org/chemcomm

Cite this: DOI: 10.1039/c0xx00000x

www.rsc.org/xxxxxx

ARTICLE TYPE

Hexaphenylbenzene based AIEE active probe for the preparation of ferromagnetic α-Fe_2O_3 nanoparticles: Facile Synthesis and catalytic applications

Subhamay Pramanik, Vandana Bhalla,* and Manoj Kumar*

Received (in XXX, XXX) Xth XXXXXXXXX 20XX, Accepted Xth XXXXXXXXX 20XX
DOI: 10.1039/b000000x

Fluorescent aggregates formed by self-assembly of hexaphenylbenzene based derivative 3 serves as reactor and stabilizer for the formation of ferromagnetic iron oxide (α-Fe_2O_3) nanoparticles in aqueous medium at room temperature. These α-Fe_2O_3 nanoparticles showed excellent catalytic activity in palladium, copper and amine free Sonogashira cross coupling reactions and also in photo catalytic degradation of Rhodamine B dye.

The development of iron oxide nanoparticles (NPs) has attracted a lot of research interest because of their potential applications in numerous areas, such as biomedicine/biotechnology,[1a] catalysis,[1b] magnetic sensors,[1c] magnetic fluids,[1d] data storage devices,[1e] magneto-optical devices,[1f] magnetic refrigeration,[1g] magnetic cell labelling,[1h] separation, tracking[1i] and drug delivery.[1j] Iron oxide nanoparticles, in combination with radiotherapy or chemotherapy are approved as a medical tool for the treatment of tumour hyperthermia in brain and prostate cancer.[2] These nanoparticles are also useful for diagnostic purposes, such as contrast agents for magnetic resonance imaging (MRI).[3] In addition, till date, there are a few reports of iron oxide nanoparticles being used as catalysts in Sonogashira[4] cross-coupling reactions replacing costly palladium, gold, silver and nickel metals. Keeping this in view, the development of new approaches for preparation of iron oxide NPs is an area of great interest. However, these iron oxide NPs have strong tendency to form aggregates and to undergo degradation when directly exposed to severe environmental conditions, hence, stability of the synthesised iron oxide NPs is an important issue. The methods already reported in the literature to enhance the stability of these magnetic nanoparticles (MNPs) suffer from the limitations of requiring longer reaction time and high temperature conditions.[5] Thus, the development of facile and rapid method for the preparation of iron oxide nanoparticles based on supramolecular aggregates at room temperature is still a challenge.

Recently, we reported the aggregates of pentacenequinone derivatives which serve as reactors for the preparation of palladium[6a] and gold nanoparticles.[6b] However, since gold and palladium metal salts are quite expensive, the preparation of nanoparticles of these metals is not economically viable. On the other hand, iron salts are very cheap in comparison to palladium and gold salts, we envisaged that if it could be possible to prepare iron based nanoparticles, these would be more attractive. Keeping this in mind, we were then interested in the development of fluorescent assemblies for the preparation of iron oxide nanoparticles at room temperature which could show excellent catalytic properties and for this purpose we designed and synthesized azaindole appended hexaphenylbenzene based compound **3**. We have chosen HPB moiety because it is known to undergo aggregation induced emission enhancement (AIEE)[7] in water to form fluorescent spherical aggregates. Further, the presence of azaindole and imino moieties at the surface of the spherical aggregates may enhance the affinity towards different soft metal ions. Interestingly, due to the presence of azaindole moieties, aggregates of **3** exhibited ratiometric response towards Fe^{3+} ions and served as reactor as well as stabilizer for the generation of ferromagnetic iron oxide NPs. To the best of our knowledge, this is the first report where the aggregates of hexaphenylbenzene derivative **3** serve as reactors for the preparation of ferromagnetic α-Fe_2O_3 nanoparticles in aqueous media at room temperature. Further, the method reported in the present manuscript for the preparation of α-Fe_2O_3 nanoparticles is better than the other methods reported in the literature (Table S1, ESI†) for the preparation of α-Fe_2O_3 nanoparticles. In addition, we believe that this is one of the best ratiometric chemosensors for Fe^{3+} ions in nanomolar range among all the chemosensors reported in the literature (Table S2, ESI†). Moreover, these α-Fe_2O_3 nanoparticles so generated showed excellent catalytic efficiency in Pd, CuI and amine free Sonogashira cross coupling reactions (Table S3, ESI†) as well as in the photo catalytic degradation of Rhodamine B dye (Table S4, ESI†). In addition, the catalytic performance of α-Fe_2O_3 nanoparticles is better than the noble metal catalysts like Pd, Au, Ag, Ru etc. used for Sonogashira coupling reported in the literature (Table S5, ESI†).

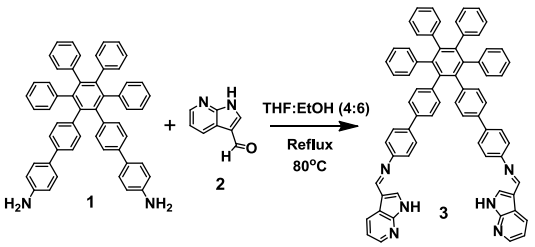

Scheme 1. Synthesis of HPB based derivative **3.**

Condensation of compound **1**[7a] with 7-azaindole-3-

carboxaldehyde, **2** furnished derivative **3** in 85% yield (Scheme 1). The structure of compound **3** was confirmed from its spectroscopic and analytical data (Fig. S26-S29, ESI†).

The UV-vis spectrum of receptor **3** in ethanol exhibits an absorption band at 320 nm due to π-π* transition. On addition of water content up to 70% (volume fraction) to the ethanol solution of **3**, the intensity of entire absorption spectra is gradually increased with the appearance of a *level-off* tail in the visible region (400-600 nm) (Fig. S1A, ESI†). The fluorescence spectrum of compound **3** in EtOH exhibits an emission band at 445 nm (Φ = 0.03) when excited at 320 nm. However, on addition of water fraction up to 70% (volume fraction) to the ethanol solution of **3**, the enhancement in the emission intensity (Φ = 0.16) is observed at 455 nm (Fig. S1B, ESI†). The quantum yield (Φ) gradually increases with increase in water fraction in the ethanol solution of **3** (Fig. S3B, ESI†). Further, an increase in fluorescence intensity of compound **3** is observed with increasing fraction of triethyleneglycol (TEG) (Fig. S3A, ESI†) and also with increasing concentration of compound **3** in ethanol (Fig. S2, ESI†). The time-resolved fluorescence studies (Fig. S4, ESI†) showed that there is very small difference between fluorescence radiative rate constants[8] (K_f) of derivative **3** in ethanol (0.15×10^9 s^{-1}) and in H_2O/EtOH (7:3, v/v) solvent mixture (0.113×10^9 s^{-1}), however, large decrease in case of non-radiative decay constant (K_{nr}) was observed from 4.85×10^9 s^{-1} to 0.59×10^9 s^{-1} (Table S6, ESI†). From these results, we conclude that the deactivation of nonradiative decay due to restriction in the intramolecular rotational relaxation of the rotors linked to the core in case of derivative **3** is the principal reason of the AIEE phenomena.

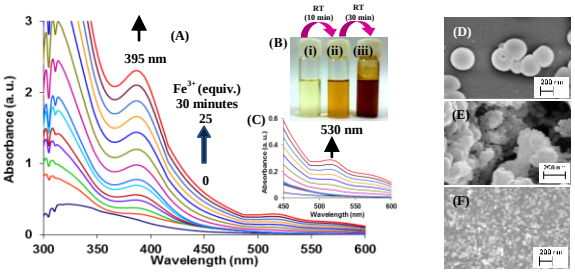

Fig. 1 (A) UV-vis spectra of aggregates of compound **3** (5 μM) in the presence of Fe^{3+} ions (0-25 equiv.) in H_2O/EtOH (7:3, v/v); (B) Naked eye colour change on addition of Fe^{3+} ions to the solution of aggregates of **3** from (i) colourless to (ii) yellow after 10 minutes and then to (iii) dark brown after 30 minutes; (C) Appearance of a new band at 530 nm; (D) SEM images of aggregates of derivative **3**; (E) SEM images of aggregates of derivative **3** after the addition of Fe^{3+} ions; (F) SEM images of separated α-Fe_2O_3 nanoparticles.

We also carried out concentration dependent ^{1}H NMR studies of derivative **3** which showed the downfield shift (δ = 0.40 ppm) of -NH protons which suggests the presence of intermolecular hydrogen bonding between the molecules. Further, an average upfield shift of 0.10 ppm was observed in case of protons corresponding to HPB moiety (Fig. S6, ESI†). Such an upfield shift of aromatic protons may be attributed to the intermolecular π-π stacking between the molecules. All these studies prove the AIEE characteristics of the derivative **3**. The SEM images (Fig. 1D) of compound **3** in H_2O/EtOH (7:3, v/v) showed the presence of spherical aggregates. The DLS studies also indicated the formation of aggregates having average diameter in the range of 300 nm (Fig. S18a, ESI†).

The presence of the imine and azaindole functionalities in the compound **3** prompted us to evaluate the binding ability of **3** toward different metal ions such as Zn^{2+}, Cu^{2+}, Hg^{2+}, Fe^{2+}, Fe^{3+}, Co^{2+}, Pb^{2+}, Ni^{2+}, Cd^{2+}, Ba^{2+}, Mg^{2+}, Ag^{+}, Al^{3+}, Ca^{2+}, K^{+} and Na^{+} as their perchlorate/chloride/or both perchlorate and chloride salts using UV-vis and fluorescence spectroscopy (Fig. S7, ESI†). Upon gradual addition of Fe^{3+} ions (0-25 equiv. within 30 minutes) to the solution of **3** (5 μM) in H_2O/EtOH (7:3, v/v), a new absorption band at 395 nm was observed (Fig. 1A).[9] These spectral changes are accompanied by color change from colourless to yellow (10 minutes) and then to dark brown (30 minutes) visible to naked eye (Fig. 1B). A new shoulder peak appeared at 530 nm along with an abrupt increase in intensity of the absorption band at 395 nm (Fig. 1C) on recording the UV-vis spectrum after 30 minutes. The shoulder at 530 nm may be attributed to a spin-forbidden 3d (Fe^{3+})→3d (Fe^{3+}) indirect transition and the band at 395 nm may be attributed to 2p (O^{2-})→3d (Fe^{3+}) direct transition i.e., charge transfer band.[10a] These spectral changes suggest the formation of α-Fe_2O_3 nanoparticle.[10b] The rate constant for the formation of nanoparticles was found to be 2.66×10^{-3} Sec^{-1} (Fig. S8, ESI†).

We also carried out pH studies to investigate the mechanism of formation of α-Fe_2O_3 nanoparticles.[11] We carried out UV-vis studies of compound **3** (5 μM) in H_2O/EtOH (7:3, v/v), in the presence of Fe^{3+} ions at different pH values and it was found that on increasing the pH from 7 to 11, the bands at 395 and 530 nm appeared quickly. These studies suggest that the formation of iron oxide nanoparticles is more favourable in basic medium (Fig. S9, ESI†).

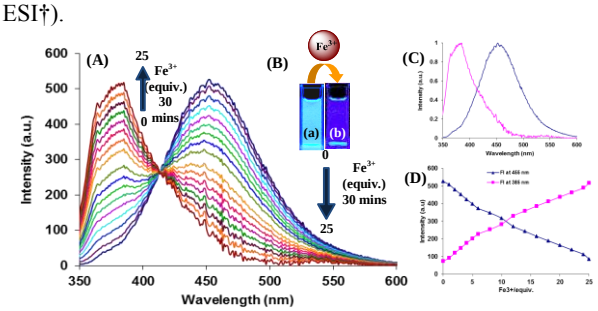

Fig. 2 (A) Fluorescence spectra of aggregates of compound **3** (5 μM) in the presence of Fe^{3+} ions (0-25 equiv.) in H_2O/EtOH (7:3, v/v) buffered with HEPES; pH = 7.05; λ_{ex}= 320 nm; (B) Colour change from (i) sky blue to (ii) violet blue after the addition of Fe^{3+} ions to the aggregates of derivative **3** (under 365 nm UV light); (C) Normalised fluorescence intensity at 455 nm and 385 nm; (D) Change in fluorescence intensity at 455 nm and 385 nm on addition of Fe^{3+} ions.

In the fluorescence spectrum, upon addition of Fe^{3+} ions to the solution of aggregates of **3**, the fluorescence maxima at 455 nm gradually decreased and a new band appeared at 385 nm with an isoemissive point at 415 nm (Fig. 2A). These spectral changes are accompanied by colour change from sky blue to violet blue visible to naked eye under 365 nm UV light (Fig. 2B). The fluorescence quantum yield of the **3** in presence of Fe^{3+} ions was found to be 0.14 (at 385 nm). Further, by considering the change in fluorescence intensity at 455 nm (I_{485}) and at 385 nm (I_{385}), 8.7 fold emission enhancement was observed at 385 nm in the case of Fe^{3+} ions. We believe that in the presence of Fe^{3+} ions, the intermolecular hydrogen bonding between azaindole moieties within aggregates of derivative **3** could be disrupted to form monomer of azaindole, responsible for the fluorescence

enhancement at 385 nm. The ratiometric response of derivative **3** towards Fe^{3+} ions was studied by fluorescence quenching efficiency plot which is linear with the increase in concentration of Fe^{3+} ions up to 16 equiv. with a Stern-Volmer constant (K_{sv}) of 6.08×10^4 M^{-1} (Fig. S10, ESI†). The detection limit was found to be 64 nM for Fe^{3+} ions (Fig. S11, ESI†). Under the same conditions as used for Fe^{3+} ions, we tested the fluorescence behaviour of aggregates of derivative **3** toward other metal ions such as Fe^{2+}, Cd^{2+}, Hg^{2+}, Pd^{2+}, Ni^{2+}, Zn^{2+}, Cu^{2+}, Co^{2+}, Ca^{2+}, Ba^{2+}, Ag^{+}, Na^{+} and K^{+} ions as their chloride and perchlorate salts, but no significant change in fluorescence intensity was observed (Fig. S12, ESI†). Thus, the aggregates of derivative **3** are selective for Fe^{3+} ions only.

We also carried out time resolved fluorescence studies of derivative **3** in presence and in the absence of ferric ions.[12] The fluorescence life time data for derivative **3** in H_2O/EtOH (7:3, v/v) was obtained by fitting the time resolved curves based on bi-exponential function at 385 nm (Fig. S13, ESI†). The half-life of excited state I (τ_1) and II (τ_2) was in the order of 0.27 and 1.55 ns. In the absence of Fe^{3+} ions, major fractions of molecules (95%) undergo radiative decay through the fast pathway (τ_1 = 0.27 ns) whereas in the presence of Fe^{3+} ions, major fractions (55%) of the molecules decay through the slower pathway (τ_2 = 1.78 ns). Moreover, both the life times τ_1 and τ_2 increased to 0.57 and 1.78 ns respectively which resulted in the large decrease in nonradiative rate constant. These results are in good agreement with the fluorescence enhancement at 385 nm (Table S7, ESI†).

The ability of the aggregates of **3** to detect Fe^{3+} ions in solid state was also investigated by preparing dip-coated paper strips in the solution of **3** on Whatman filter paper followed by drying the strips under vacuum. Fluorescence change from sky blue to dark blue was observed under UV lamp of 365 nm light upon dipping the test strips into aqueous solutions of $FeCl_3$ (Fig. S14A, ESI†). This result validates the utility of the test strips for the instant visualization of traces of Fe^{3+} ions. Dark blue fluorescent spots of different intensities were observed by varying the concentration of Fe^{3+} ions even up to the level of 10^{-6} M (Fig. S14B, ESI†). These results indicate that **3** can detect Fe^{3+} ions in aqueous media at very low concentration.

To get further insight into the mechanism of formation of iron oxide nanoparticles, we slowly evaporated the solution of aggregates of derivative **3** containing nanoparticles. After 2 days, precipitates were obtained which were filtered and washed with THF. The ^{1}H NMR spectrum of the residue (Fig. S15, ESI†) so obtained after evaporation of THF solution showed the upfield shift of 0.44, 0.31 and 0.40 ppm for NH, imino and aromatic protons respectively (Table S8, ESI†). On the basis of above results we believe that upon addition of Fe^{3+} ions to the solution of aggregates of **3**, Fe^{3+} ions interact with nitrogen atoms of compound **3** to enter into the network of interconnected channels and get reduced to Fe(0) which is further oxidised to stable α-Fe_2O_3 by up taking oxygen from water. Thus, aggregates of derivative **3** functions as reactor and stabilizing agent for the preparation of nanoparticles at room temperature. The SEM image of derivative **3** in presence of Fe^{3+} ions in H_2O/EtOH (7:3, v/v) solution showed the formation of iron oxide nanoparticles on the surface of the aggregates of **3** (Fig. 1E and S16A, ESI†). Further, the SEM images (Fig. 1F) of the residue show the formation of very smaller iron oxide nanoparticles. The powder X-ray diffraction (XRD) studies[13] of the precipitates showed the presence of diffraction peaks located at 2θ values of 24.17, 33.20, 35.68, 40.91, 49.49, 54.12, 62.48, 64.03, 73.02 & 75.14 which suggest the formation of α-Fe_2O_3 nanoparticles (Fig. S17A, ESI†). The result of energy dispersive X-ray (EDX) confirmed that the iron oxide precursor consisted of iron and oxygen, a chemical composition that agreed well with the formation of α-Fe_2O_3 nanoparticles (Fig. S17B, ESI†). The TEM images of derivative **3** in presence of Fe^{3+} ions revealed that the formation of nanorods of average length 12-18 nm (Fig. S16B, ESI†). The DLS studies showed the formation of α-Fe_2O_3 nanoparticles having average diameter in the range of 4-6 and 10-18 nm nanoparticles (Fig. S18b, ESI†). The IR spectrum of these nanoparticles exhibit strong bands in the low frequency region (700-350 cm^{-1}) due to iron oxide architecture (Fig. S19, ESI†).[14] The magnetic hysteresis measurements of the typical nanorods of α-Fe_2O_3 were carried out at 300 K with the applied magnetic field sweeping from -20 to +20 kOe (Fig. S20, ESI†).[15] The magnetic hysteresis loops of the typical α-Fe_2O_3 show ferromagnetic behavior with a remnant magnetization (M_r) of 0.20 emu g^{-1} and coercivity force (H_c) of 1828.68 Oe.

To investigate the catalytic efficiency of α-Fe_2O_3 nanoparticles so generated, we studied the photo catalytic degradation of Rhodamine B (RhB, 0.1 mM) dye and C-C bond forming Sonogashira cross coupling in the presence of these nanoparticles. We have carried out photo catalytic degradation of the aqueous solution of RhB dye in the presence of 2 mM H_2O_2.[16] The progress of degradation was monitored by observing the change in intensity of the characteristic absorption peak of RhB at 555 nm (Fig. S21A, ESI†). The absorption spectrum of RhB solution showed time-dependent change in the presence of α-Fe_2O_3 nanoparticles (2 μM) under visible-light irradiation. The characteristic absorption peak of RhB at 555 nm rapidly decreased in intensity as time prolonged and it disappeared completely after about 26 minutes and the color of the solution changed from the initial pink-red to almost colourless (Fig. S21A, ESI†). The rate constant for photo catalytic degradation of aqueous RhB dye by α-Fe_2O_3 was found to be 1.79×10^{-3} Sec^{-1} (Fig. S21B, ESI†).

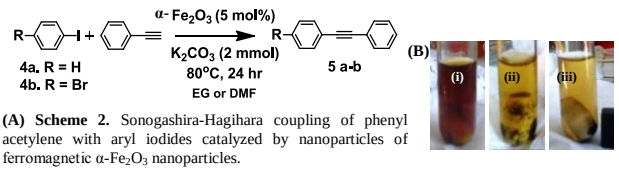

(A) Scheme 2. Sonogashira-Hagihara coupling of phenyl acetylene with aryl iodides catalyzed by nanoparticles of ferromagnetic α-Fe_2O_3 nanoparticles.

Fig. 3 (A) Scheme 2; (B) α-Fe_2O_3 nanoparticle (i) dispersed in the reaction mixture; (ii) adsorbed on magnetic stirring bar; (iii) an external magnet attracted stirring bar and α-Fe_2O_3 nanoparticles.

In addition, we also carried out Sonogashira cross coupling of aryl-iodides (4a-b) and phenyl acetylene in the presence of these nanoparticles to yield the desired products in high yields within 24 hours as shown in Fig. 3A, Scheme 2 (Table S9, ESI†). The products (5a-b) were isolated and characterized by ^{1}H NMR, ^{13}C NMR and ESI-MS (Fig. S22-S25, ESI†). The catalytic efficiency of these α-Fe_2O_3 nanoparticles is comparable/better than the existing Pd-based catalysts for the mentioned Sonogashira coupling reactions (Table S10a-10b, ESI†). The ferromagnetic α-

Fe_2O_3 nanoparticles could be easily separated from the reaction mixture by the magnet and the separated catalysts could be recycled for 5 consecutive times without significant loss of its activity (Fig. 3B). The separation and reuse of the ferromagnetic α-Fe_2O_3 nanoparticles was very simple, effective and economical. The desired product was not obtained in the absence α-Fe_2O_3 nanoparticles.

In conclusion, we designed and synthesized hexaphenylbenzene derivative **3** having azaindole groups which forms fluorescent aggregates in aqueous media. These aggregates show high affinity towards Fe^{3+} ions in nanomolar range. Interestingly, these aggregates of **3** serve as reactors and stabilizer for the preparation of ferromagnetic α-Fe_2O_3 nanoparticles at room temperature within 30 minutes. Further, these α-Fe_2O_3 nanorods show excellent catalytic activity of in Sonogashira cross coupling reactions and in photo catalytic degradation of RhB dye.

M.K. and V. B. are thankful to DST (ref no. SR/S1/OC-69/2012) and CSIR (ref. no. 02(0083)/12/EMR-II) respectively for financial support. We are also thankful to UGC (New Delhi) for "University with Potential for Excellence" (UPE) project. S.P. is thankful to UGC (New Delhi) for Senior Research Fellowship (SRF).

Notes and references

Department of Chemistry, UGC Sponsored Centre for Advanced Studies-1, Guru Nanak Dev University, Amritsar-143005, Punjab, India.

E-mail: vanmanan@yahoo.co.in, mksharmaa@yahoo.co.in

† Electronic Supplementary Information (ESI) available: [Experimental detais, NMR and Mass Spectra,]. See DOI: 10.1039/b000000x/

1 (a) F. Hu, L. Wei, Z. Zhou, Y. Ran, Z. Li and M. Gao, *Adv. Mater.*, 2006, **18**, 2553; (b) C. -H. Jun, Y. J. Park, Y. -R. Yeon, J. -R. Choi, W. -R. Lee, S. -J. Ko and J. Cheon, *Chem. Commun.*, 2006, 1619; (c) D. J. Sellmyer, *Nature*, 2002, **420**, 374; (d) U. Jeong, X. Teng, Y. Wang, H. Yang and Y. Xia, *Adv. Mater.*, 2007, **19**, 33; (e) C. T. Black, C. B. Murray, R. L. Sandstrom and S. Sun, *Science*, 2000, **290**, 1131; (f) R. F. Ziolo, E. P. Giannelis, B. A. Weinstein, M. P. O'Horo, B. N. Ganguly, V. Mehrotra, M. W. Russell and D. R. Huffman, *Science*, 1992, **257**, 219; (g) O. Tegus, E. Br¨uck, K. H. J. Buschow and F. R. de Boer, *Nature*, 2002, **415**, 150; (h) M. Lewin, N. Carlesso, C. H. Tung, X. W. Tang, D. Cory, D. T. Scadden and R. Weissleder, *Nat. Biotechnol.*, 2000, **18**, 410; (i) D. S. Wang, J. B. He, N. Rosenzweig and Z. Rosenzweig, *Nano Lett.*, 2004, **4**, 409; (j) M. Namdeo, S. Saxena, R. Tankhiwale, M. Bajpai, Y. M. Mohan and S. K. Bajpai, *J. Nanosci. Nanotechnol.*, 2008, **8**, 3247.

2 M. Johannsen, B. Thiesen, P. Wust and A. Jordan, *Int. J. Hyperthermia*, 2010, **26**, 790.

3 J. R. McCarthy and R. Weissleder, *Adv. Drug Delivery Rev.*, 2008, **60**, 1241.

4 H. Firouzabadi, N. Iranpoor, M. Gholinejad and J. Hoseinib, *Adv. Synth. Catal.*, 2011, **353**, 125.

5 Yong Li and Wenjie Shen, *Chem. Soc. Rev.*, 2014, **43**, 1543.

6 (a) V. Bhalla, A. Gupta and M. Kumar, *Chem. Commun.*, 2012, **48**, 11862; (b) K. S. nee Kamaldeep, S. Kaur, V. Bhalla, M. Kumar and A. Gupta, *J. Mater. Chem. A*, 2014, **2**, 8369.

7 (a) V. Bhalla, S. Pramanik and M. Kumar, *Chem. Commun.*, 2013, **49**, 895; (b) Y. Hong, J. W. Y. Lam and B. Z. Tang, *Chem. Soc. Rev.*, 2011, **40**, 5361.

8 (a) Y. Kubota, S. Tanaka, K. Funabiki and M. Matsui, *Org. Lett.*, 2012, **14**, 4682; (b) Y. Ren, J. W. Y. Lam, Y. Dong, B. Z. Tang and K. S. Wong, *J. Phys. Chem. B*, 2005, **109**, 1135.

9 J. Lian, X. Duan, J. Ma, P. Peng, T. Kim and W. Zheng, *ACS Nano*, 2009, **3**, 3749.

10 (a) M. Diab and T. Mokari, *Inorg. Chem.*, 2014, **53**, 2304; (b) S. Li, W. Yan and W. Zhang, *Green Chem.*, 2009, **11**, 1618.

11 I. Kazeminezhad and S. Mosivand, *Acta Phys. Pol., A*, 2014, **125**, 1210.

12 C. Karunakaran, J. Jayabharathi, R. Sathishkumar and K. Jayamoorthy, *Spectrochim. Acta, Part A*, 2013, **110**, 151.

13 (a) Y. -P. Sun, X. -Q. Li, J. Cao, W. -X. Zhang and H. P. Wang, *Adv. Colloid Interface Sci.*, 2006, **120**, 47; (b) J. Chen, L. Xu, W. Li and X. Gou, *Adv. Mater.*, 2005, **17**, 582.

14 S. Yu and G. M. Chow, *J. Mater. Chem.*, 2004, **14**, 2781.

15 S. Yang, Y. Xu, Y. Sun, G. Zhang and D. Gao, *Cryst. Eng. Commun.*, 2012, **14**, 7915.

16 G. Liu, Q. Deng, H. Wang, D. H. L. Ng, M. Kong, W. Caia and G. Wang, *J. Mater. Chem.*, 2012, **22**, 9704.